Climatology of global, hemispheric and regional electron content variations during the solar cycles 23 and 24

Waqar Younas, Christine Amory-Mazaudier, Majid Khan, Paul O Amaechi

Available online at www.sciencedirect.com

ScienceDirect

Advances in Space Research xxx (xxxx) xxx

ADVANCES IN SPACE RESEARCH (a COSPAR publication)

www.elsevier.com/locate/asr

Climatology of global, hemispheric and regional electron content variations during the solar cycles 23 and 24

Waqar Younas [a], C. Amory-Mazaudier [b,c], Majid Khan [a,*], Paul O. Amaechi [d]

[a] Department of Physics, Quaid-i-Azam University, Islamabad 45320, Pakistan

[b] Sorbonne Université, Ecole polytechnique, Institut Polytechnique de Paris, Université Paris Saclay, Observatoire de Paris, CNRS, Laboratoire de Physique des Plasmas (LPP), 75005 Paris, France

[c] The Abdus Salam International Centre of Theoretical Physics, Trieste, Italy

[d] Cardiff School of Education & Social Policy, Cardiff Metropolitan University, Cyncoed Campus, Cardiff, UK

Received 15 November 2021; received in revised form 13 May 2022; accepted 12 July 2022

Abstract

We present the results of study on the variations of ionospheric total electron content (TEC) by using global, hemispheric, and regional electron contents computed from the global ionospheric maps (GIMs) for the period from 1999 to 2020. For a low and moderate solar activity, the global and regional electron contents vary linearly with solar 10.7 cm radio flux and EUV flux. While a saturation effect in the electron content verses EUV and F10.7 is found during the high solar activity periods at all regions, the maximum effect is observed at low-latitudes followed by high and mid-latitudes region. The extent of saturation effect is more pronounced for F10.7 as compared to EUV. A wavelet transform is applied to global and hemispheric electron contents to examine the relative strength of different variations. The semi-annual variations dominate in the northern hemisphere, whereas annual variations dominate in the southern counterpart. The amplitude of annual variations in southern hemisphere is found to be higher than northern counterpart at all latitudes. This asymmetry in the amplitude of annual variation is maximum at low-latitudes, followed by mid and high-latitudes, respectively. The semi-annual variations are in-phase in both hemisphere and follow the solar cycle. The northern hemisphere depicts relatively large amplitude of semi-annual variations and exhibit the maximum effect at high-latitudes.

Keywords: Total electron content; Ionosphere; Global electron content; Annual variation; Semi-annual variation

1. Introduction

The ionosphere is an ionized part of the Earth's upper atmosphere, formed by absorption of extreme ultraviolet radiations (EUV). Space weather activities such as coronal mass ejection (CME), solar flares and tides in the lower atmosphere also contribute to the variability of ionosphere (Rishbeth, 1998; Rishbeth, 2006). The ionospheric plasma density exhibits several periodic variations like diurnal, 27-days, seasonal and solar cycle. Furthermore, the ionosphere also exhibits anomalous behavior, deviating from the predictions of Chapman ionization theory. The prominent anomalies include winter anomaly, equatorial anomaly, annual and semi-annual anomalies (Rishbeth, 1998).

Annual anomaly, otherwise known as the annual asymmetry or annual variation, refers to the higher (approximately 30%) plasma densities near December solstice than near June solstice (Rishbeth and Müller-Wodarg, 2006). The mechanism for annual variation is not properly understood and listed as one of the top scientific challenges in the ionospheric research (Rishbeth, 2007). Berkner and

* Corresponding author.
E-mail address: majid.khan@qau.edu.pk (M. Khan).

https://doi.org/10.1016/j.asr.2022.07.029
0273-1177/

Wells (1938) first reported the annual asymmetry and later studies by Rishbeth and Müller-Wodarg (2006) ionosondes measurements and Mendillo et al. (2005) via GPS-TEC analysis. Later, Zeng et al., (2008) investigated the features of annual variation using the COSMIC radio occultation technique and compared the results with TIEGCM model. They showed that the annual asymmetry varies strongly with local time and longitude. Rishbeth and Müller-Wodarg (2006) performed the model simulation of annual asymmetry using coupled thermosphere ionosphere plasmasphere electrodynamics (CTIPe) model. The said model provides much lower magnitude of the annual asymmetry as compared to observational data. This indicates that several other ionizing sources need to be taken into account. Dang et al. (2017) performed numerical simulations of the annual asymmetry using NCAR-TIEGCM model and found that such annual variation is mainly dependent on the distance between Sun and Earth through photochemical process. The winter anomaly refers to daytime plasma density higher in winter than summer during same solar activity (Torr and Torr, 1973; Zou et al., 2000, Burns et al. 2014).

The semi-annual variation refers to higher plasma density at equinox than solstice. Many theories have been proposed to explain the semi-annual anomaly as reviewed by Rishbeth (1998). Cortie (1912) proposed that solar wind speed is high near equinox as compared to solstice and this may be origin of semi-annual variation. Thermometric spoon mechanism was suggested to explain these variations, which indicated that inter-hemispheric circulation in solstices plays a key role in the mixing of major plasma species. Later, Rishbeth et al. (2000) gave a detailed discussion of the said subject and role of other mechanisms in explaining the semi-annual variation. Enhanced reconnection between interplanetary and Earth's magnetic fields during the equinox season as compared to solstice is another mechanism possible for semi-annual variation (Russell and McPherron, 1973). McIntosh (1959) and Bartels (1932) proposed a Kelvin-Helmoltz type instability which is maximum at equinox. Zhao et al. (2007) studied the various characteristics of semi-annual variation using the global ionospheric maps (GIMs) and TIMED-GUVI based O/N_2 data. They also pointed out the role of thermospheric wind and electric fields for explaining the semi-annual variation. Currently, a worldwide network of dual frequency GPS receivers (https://igs.org/network/) is used to monitor the ionosphere, study its global and regional features (Unnikrishnan et al., 2002; Wu et al., 2004; Zhao et al., 2007). In the present work, we have computed the global and hemispheric electron content (Afraimovich et al., 2006; Ratovsky et al., 2020) using UPC-UQRG GIMs from 1998 to 2020. The regional electron content (REC) has also been computed at different latitudinal zones, namely low-latitudes (0°–30°), mid-latitudes (30°–60°) and high-latitudes (60°–87.5°). Finally, features of annual and semi-annual variation are investigated by applying the band-pass filters.

Rest of the articles is organized as follows: section 2 describes the data sets and methodology employed in this work. The results are presented in the section 3 while section 4 describes the discussion of our results. The conclusions are summarized in the section 5.

2. Data sets and data processing

2.1. Data sets

We have used global ionospheric maps (GIMs) as provided by UMPC to extract vertical total electron content (vTEC). These maps have a spatial resolution of 2.5° along latitude and 5.0° along longitude with temporal resolution of 15 min. Hence, there are 72x72 = 5140 data points in each GIM map, called a GIM cell. Fig. 1 depicts an example of receiver locations listed in the header information of the UQRG-IONEX file of 2014-01-01. Although the distribution of GPS stations is sparse in the southern hemisphere as compared to the northern counterpart (Fig. 1). However, during the geomagnetically quiet-days the performance of UPC-UQRG GIMs over the oceans (particularly in the southern hemisphere) shows a good agreement with satellite measurements (Jee et al., 2010; Liu et al., 2021). Hence, it provides a possibility to perform our statistical analysis for various features of the ionosphere using GIMs. We used GIM data of solar cycles 23 (SC-23) and 24 (SC-24). Solar cycle 24 is the smallest solar cycle since 1957. The year 2008 has the smallest solar activity, and the year 2009 has the smallest magnetic activity in the last one century (Zerbo et al., 2012). The period between 2006 and 2008 is known as deep solar minimum. Different phases of solar cycles 23 and 24 are depicted in Table 1. The solar EUV fluxes in range 0.1–50 nm are continuously measured by the Solar EUV Monitor (SEM) spectrometer aboard the Solar Heliospheric Observatory (SOHO) since 1996 (Judge et al.,1998). Monthly averaged EUV flux and F10.7 index have been used in this work to find their correlation with electron content variations.

2.2. Data processing

To understand variation in ionospheric electron density the global electron content (GEC), hemispheric electron content (HEC) and regional electron content (REC) are computed. Here, GEC, HEC and REC are, respectively, the number of electrons in the whole ionosphere, hemisphere and at specific latitudinal regions. All of these parameters are measured in the units of GECU such $1 GECU = 10^{32}$ electrons. The HEC is calculated by multiplying $vTEC$ value of each GIM cell $I_{p,q}$ with corresponding area $A_{p,q}$ and then summing over the entire hemisphere (Afraimovich et al., 2006, Ratovsky et al., 2020), i.e.

$$HEC = \sum_{p,q} I_{p,q} A_{p,q} \quad (1)$$

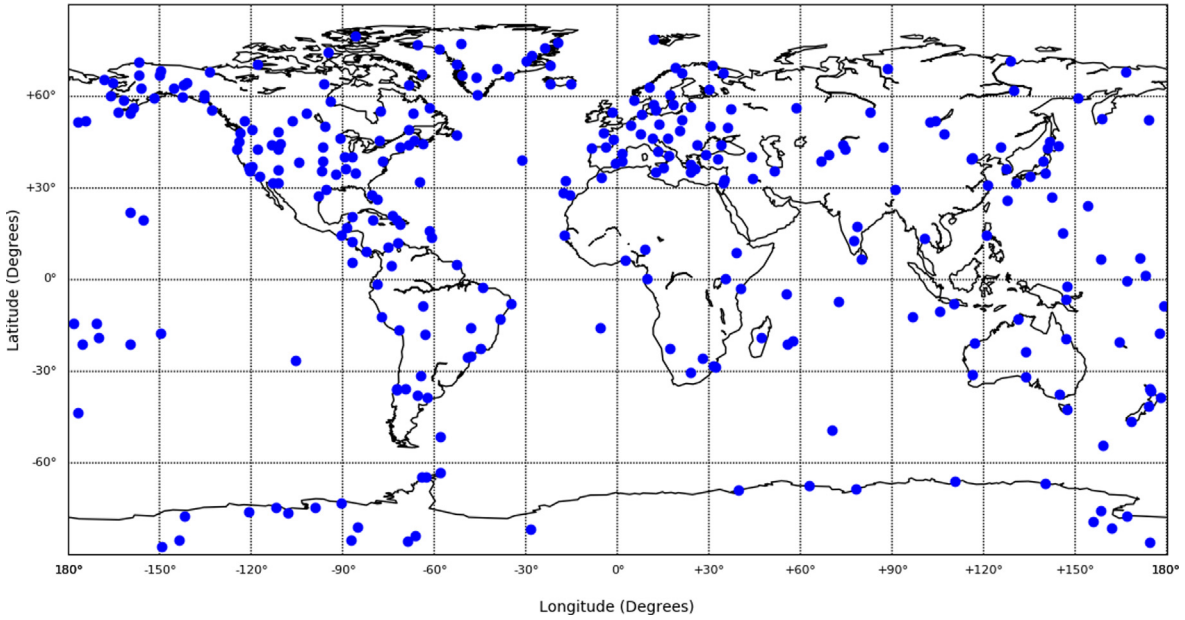

Fig. 1. GNSS receiver stations used for the UPC-UQRG ionospheric maps of 2014-01-01.

Table 1
Characteristics of solar cycles 23 and 24.

Phase	Years of SC-23	Years of SC-24
Increasing	1997 to 1999	2009 to 2011
Maximum	2000–2002	2012–2014
Decreasing	2003 to 2005	2015 to 2018
Minimum	2006 to 2008 Deep solar minimum	2019 to 2020

Here p and q denote, respectively the geographic latitude and longitude of a particular GIM cell. For northern hemispheric electron content (HEC_N), p ranges from 0° to 87.5° and for southern hemispheric electron content (HEC_S) p = -87.5° to 0° whereas q = –180° to +180° during both cases. The GEC is computed by summing the HEC, i.e., $GEC = HEC_N + HEC_S$. Whereas the REC at low, mid and high-latitudes is computed by limiting the p (Eq. (1)) to 0°–30°, 30°–60° and 60°–87.5°, respectively.

Monthly averaged values of electron contents are evaluated by using five quietest days of each month. A morlet wavelet transform has been applied to GEC and HEC to analyze strength of different oscillations (Rösch and Schmidbauer, 2016). The annual variations in electron content have a period of 12 months, whereas semi-annual variations correspond to oscillations with 6 months periodicity. A finite impulse response band-pass filter has been employed to separate such variations. The upper and lower frequency bound for annual (semi-annual) variations were 1/11 (1/6.5) months and 1/13 (1/5.5) months, respectively.

3. Results

3.1. The GEC, HEC and REC variation

Fig. 2(a) presents the average monthly GEC, in Fig. 2(b) we have shown the HEC at northern (red) and southern hemisphere (black), Fig. 2 (c) presents yearly averaged differences in the hemispheric electric content and Fig. 2(d) depicts the respective SSN (in blue) with F 10.7 (in red) superimposed on it, from the year 1999 to 2020. The GEC has a maximum value of 3.3410 GECU in the month of October 2001 and a minimum 0.4515 GECU in July 2009. The values of GEC are in agreement with finding of Astafyeva et al. (2007). During the SC-23, however, the GEC is in general relatively higher than during the SC-24, and in particular, the maximum GEC is greater by 34%. The HEC_N shows a maximum value of 1.687 GECU in March 2002, whereas the respective value southern hemisphere observed in October 2001 is 1.704 GECU. Fig. 2(c) indicates that yearly averaged HEC is high in northern hemisphere for all years except 2011, where almost equal electron contents are found in both hemispheres. The R (SSN) showed two peaks during the SC-23 maximum with peak values of 256 and 249, respectively in July 2000 and September 2001. For the cycle 24 it reaches a maximum value of 160 in February 2014. Fig. 3(a) presents REC at high-latitudes (60:87.5) from 1999 to 2020 in both hemispheres, it shows two peaks corresponding to solar cycle maximum. The REC values at high latitudes are much smaller than mid and low-latitudes. Moreover the hemispheric differences are higher during the maximum phase of a solar cycle than during the minimum phase. During December 2011, the REC in the southern high-latitudes is about 334% higher than northern counterpart. Fig. 3(b) is similar to Fig. 3(a) but for the mid-latitudes. Fig. 3(c) presents regional electron content at low-latitudes (0:30) in the northern (red) and southern hemisphere (blue) from 1999 to 2020. It can be observed that REC shows two peaks corresponding to solar maximum with maximum of 1.085 GECU (1.102

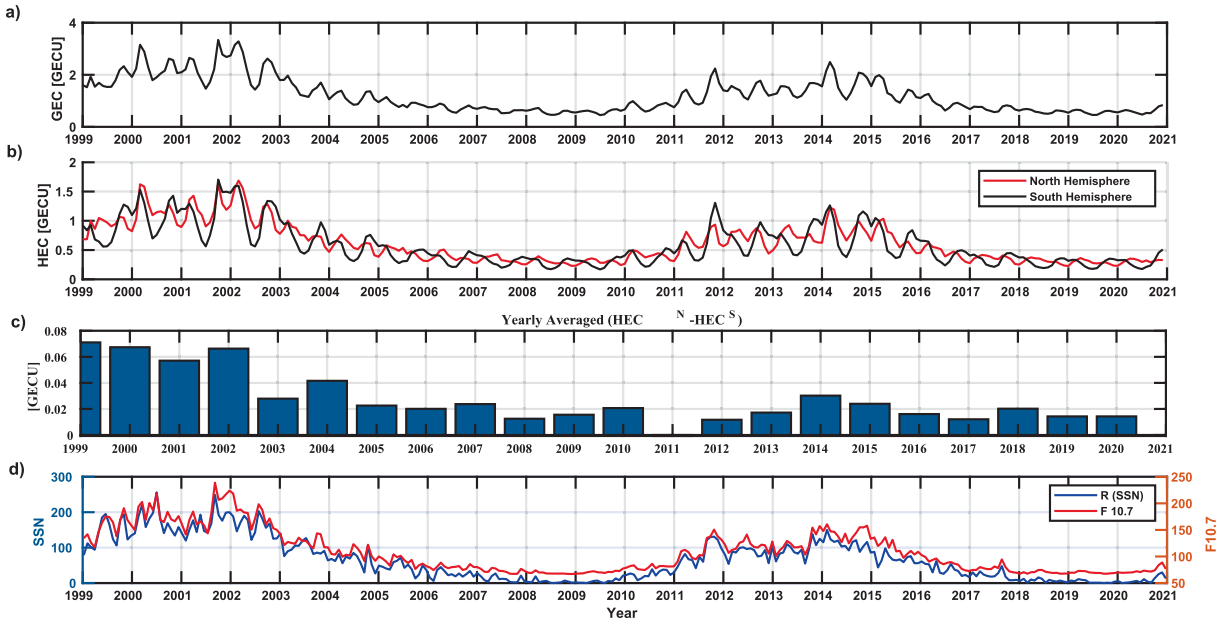

Fig. 2. **a)** Global electron content in GECU from January 1999 to December 2020 **b)** Hemispheric electron content in northern hemisphere (red) and southern hemisphere (black) from 1999 to 2020 **c)** Difference in yearly averaged hemispheric electron content **d)** Solar radio flux F10.7 (in red) and Sun spot number, R (in blue) from 1999 to 2020.

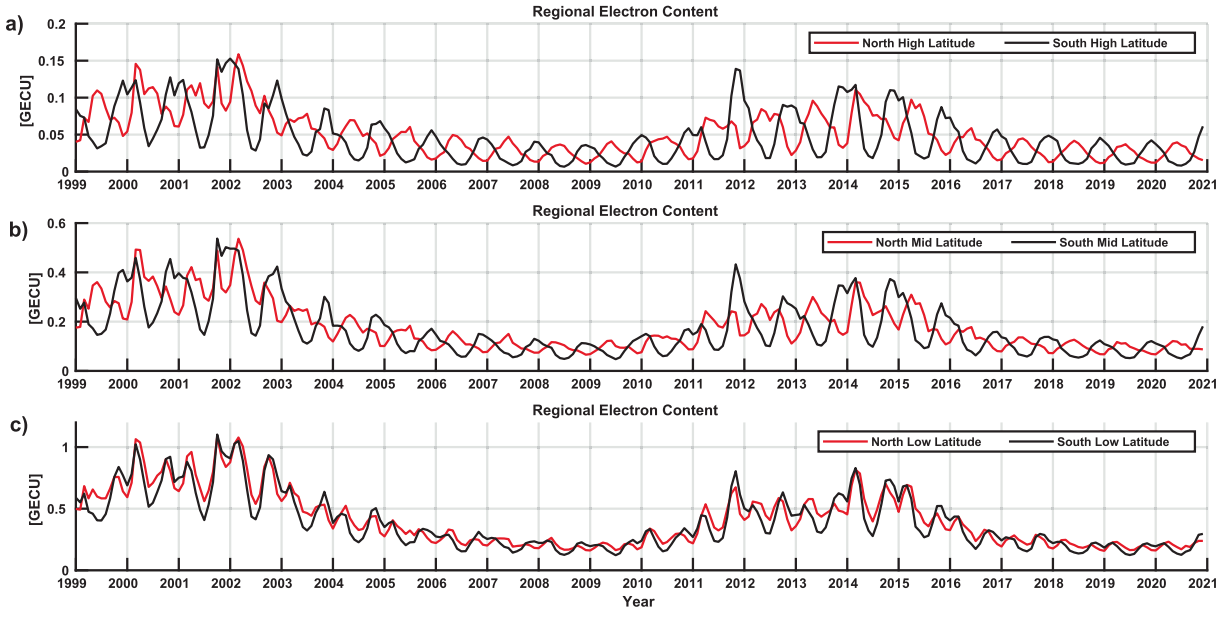

Fig. 3. **a**) Regional electron content at northern (in red) and southern (in black) high-latitudes from 1999 to 2020. **b**) Same as Fig. 3 (a) but for mid-latitudes c) same as Fig. 3(a) but for low-latitudes.

GECU) and 0.8301 GECU (0.8160 GECU) in the northern (southern) hemisphere during the months of October 2001 and March 2014, respectively.

The hemispheric differences in yearly averaged regional electron content for high, mid and low-latitudes is presented in Fig. 4a, 4b and 4c, respectively. The northern high latitude is found to have higher electron content as compared to southern counterpart for all years except during the period 2011–2013 and 2019. The mid-latitude region also exhibits higher electron content in the northern hemisphere for all years except for the period 2011–2013 and 2003. Contrary to high and mid-latitude regions, the northern low-latitude exhibits higher electron content for all years. The intensity of hemispheric asymmetry at low-latitude follows the solar cycle and depicts two peaks corresponding to maximum of solar cycles 23 and 24, respectively.

A wavelet transform is applied to global and hemispheric electron contents and its power spectrum is displayed in Fig. 5: from top to bottom we present GEC,

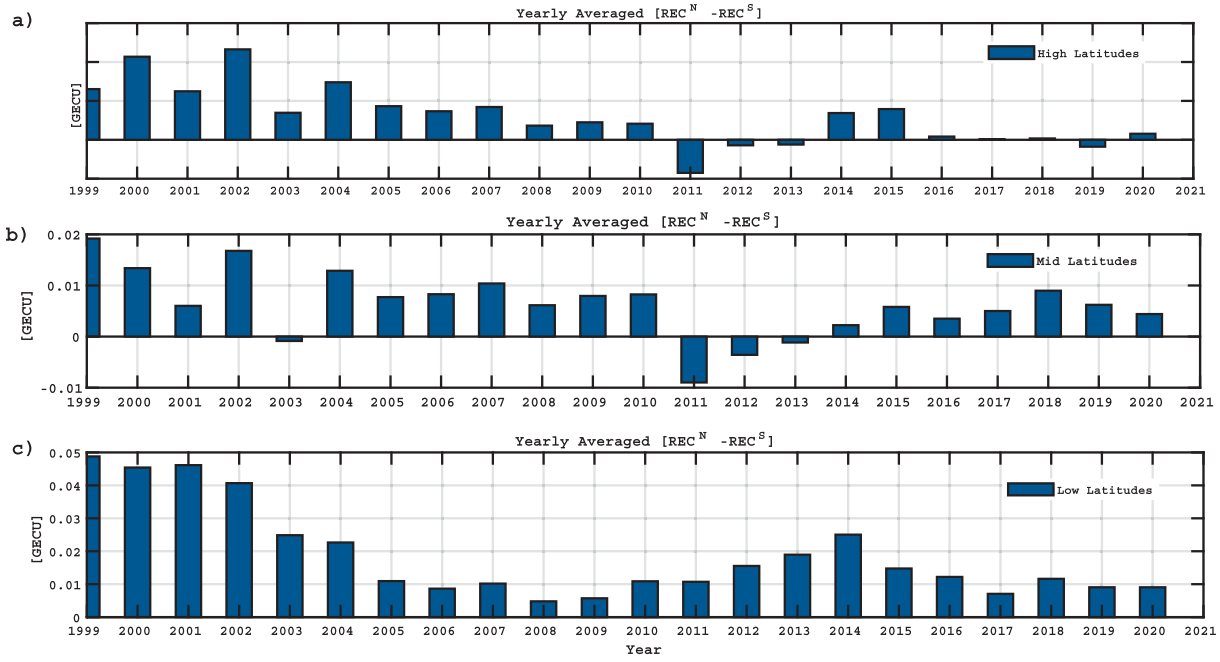

Fig. 4. Hemispheric difference in yearly averaged regional electron content for **a)** low **b)** Mid and **c)** High-latitudes region from 1999 to 2020.

HEC_N and HEC_S, respectively. Power spectrum highlights various common features during the considered interval. The first characteristic is the increase in the strength of periods between 5 months to 7 months corresponding to semi-annual variations. A second characteristic is evident increase in the power of periods between 11 month and 13 months corresponding to annual oscillations around the maximum phase of solar cycles 23 and 24. We also observe the oscillations with 32-month periodicity whose power is intensified around the solar maximum. The power spectrum of GEC reveals that annual and semi-annual component during the maximum phase of SC-23 is stronger than corresponding phase of SC-24. Another interesting feature revealed by power spectrum is semi-annual variation is most dominating component in the northern hemisphere whereas annual variation dominates in the southern counterpart.

3.2. Morphology of annual variations

In the previous section, it has been found that annual variations are one of the main oscillations in the GEC and HEC data. The present section provides a detailed analysis of annual variation in each hemisphere at different latitudinal zones. To quantify the amplitude of the annual variations a band pass filter is applied to HEC and the results are presented in Fig. 6a, orderly for northern (red) and southern hemispheres (blue) for the period 1999 to 2020. The annual variation in the northern hemisphere is relatively weaker than southern counterpart and do not follow the solar cycle trend exactly as they do for the southern hemisphere. Furthermore, the annual variation in the northern hemisphere gets stronger during the years 2010 to 2015. Whereas these variation in the southern hemisphere follow the solar cycle trends. There are two periods of strong annual variation in the southern hemisphere corresponding to maximum of 23rd and 24th solar cycles. The maximum amplitude of annual variation in the southern hemisphere found 0.3539 GECU in the month of Dec 2002 whereas in the northern hemisphere it was 0.0822 GECU in May 2012. The maximum amplitude of annual variations in the northern hemisphere is about 76% lower than southern counterpart. The amplitude of annual variation in the southern hemisphere reaches to a minimum value (about 0.1234 GECU) in 2009 whereas northern counterpart depicts a minimum value (about 0.0158 GECU) of annual variations in the month of May 2004. For the period 2000 to 2004 the annual variation in the southern hemisphere is relatively strong as compared to the corresponding values for years 2012 to 2016. The annual variations in both hemispheres are found to be out of phase. The maxima of such variations in the northern (southern) hemisphere are observed in June (December), whereas minima are observed in the month of December (June). This indicates that the annual variations as shown in Fig. 6 (a) correspond to regular annual variations in agreement with Chapman's theory (Chapman, 1931). To further investigate the features of annual variations, we have computed December to June ratio of monthly averaged electron content for GEC and HEC and results are presented in the Fig. 7. The ratio corresponds to winter anomaly (regular annual variations) if greater (less) than unity in the northern (southern) hemisphere. Fig. 7(a) indicates that GEC(Dec)/GEC(June) is maximum (1.8) in the year 2011 whereas corresponding minimum value (0.93) occurs in the year 2015. The Dec(lo-

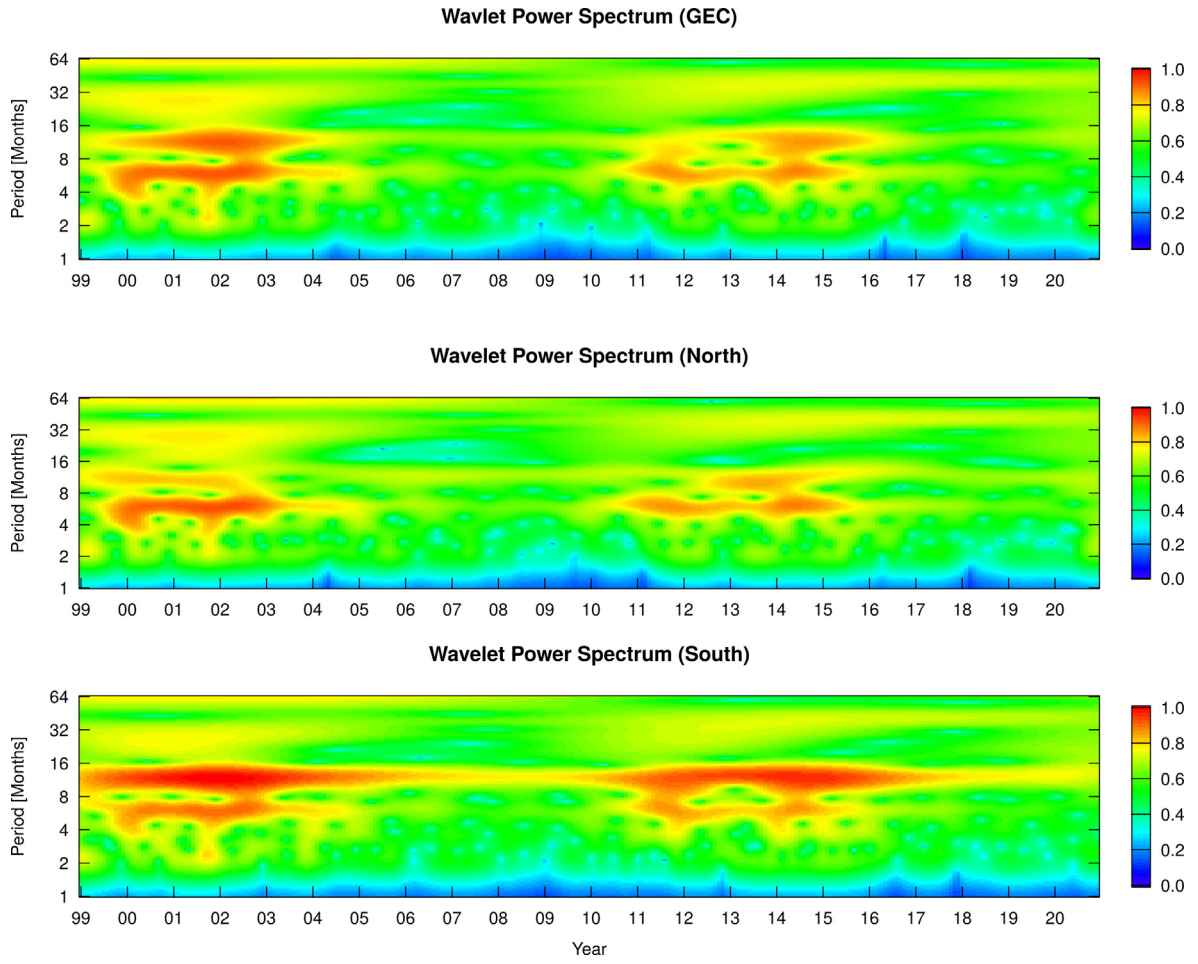

Fig. 5. Wavelet power spectrum of GEC (top), HEC_N (middle) and HEC_S (bottom) from 1999 to 2020.

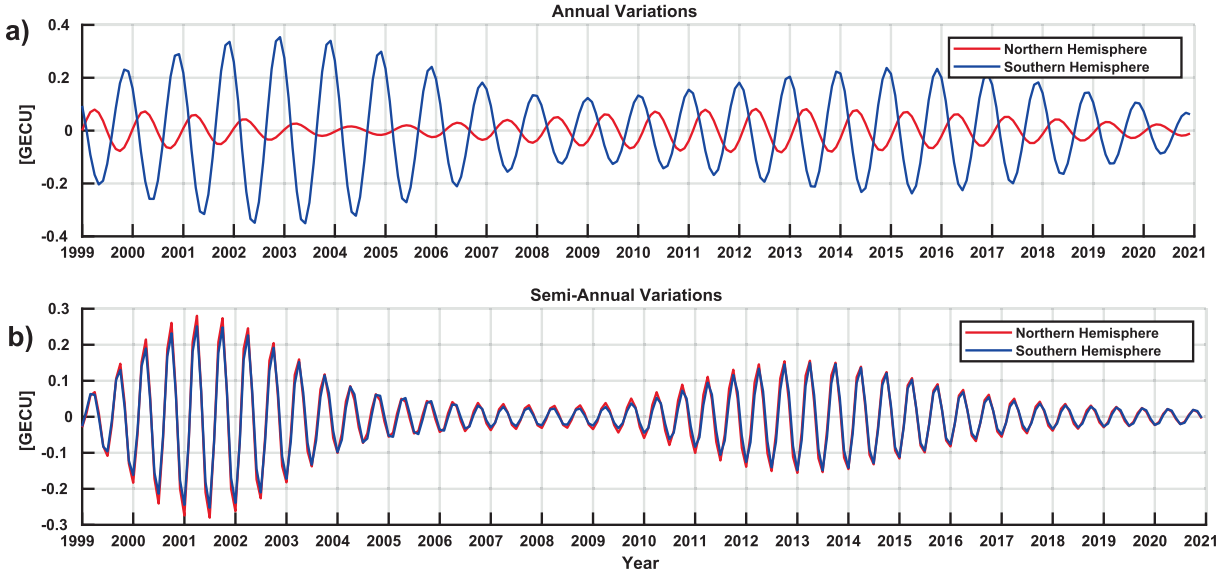

Fig. 6. **a)** Annual variation in the hemispheric electron content, red presents the north and blue corresponds to southern hemisphere **b)** Semi-annual variation in the hemispheric electron content, red presents the north and blue corresponds to southern hemisphere.

cal winter)/June (local summer) ratio for northern hemisphere is presented in Fig. 7(b), it indicates that ratio remain less than unity except during the years 2001 and 2011 where it was slightly higher than unity (1.097 and 1.037). On the other hand, in the southern hemisphere (Fig. 7(c)) Dec(local summer)/Jun (local winter) ratio

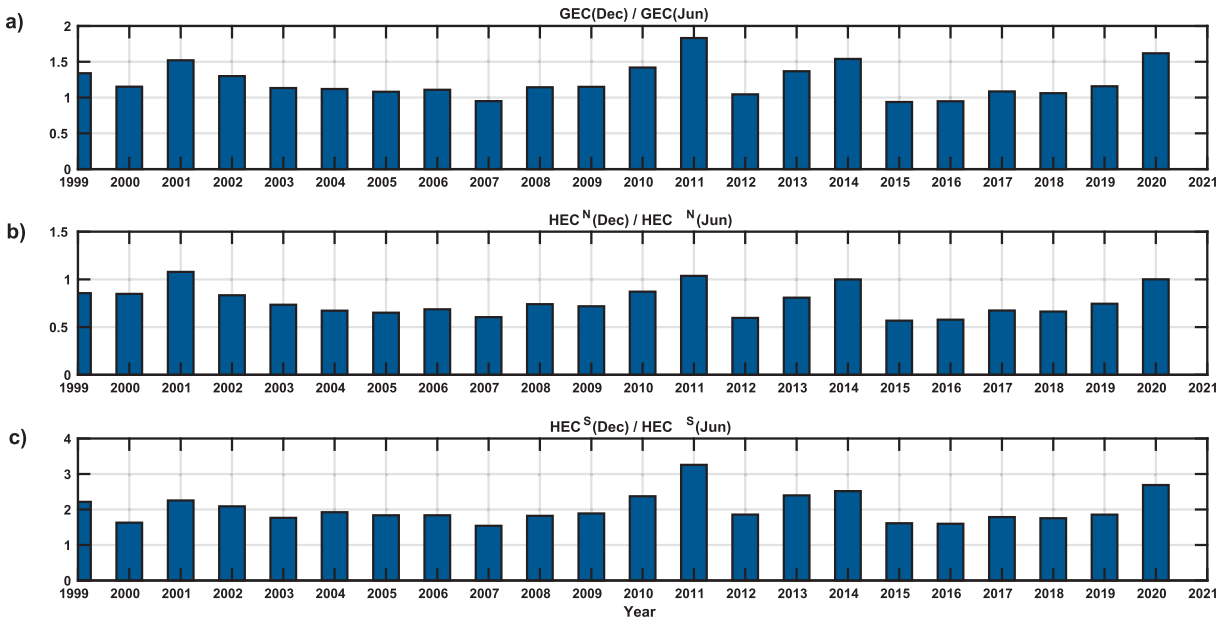

Fig. 7. **a)** December to June ratio of GEC from 1999 to 2020 **b)** same as Fig. 7(a) but for HEC_N **c)** same as Fig. 7(a) but for HEC_S.

remain greater than unity for all years with the maximum (minimum) ratio observed the year 2011 (2007) having values of 3.2(1.5), respectively.

The annual variations at high, mid and low-latitudes are extracted using a band pass filter and presented in Fig. 8(a), 8(b) and 8(c) respectively. On each panel red line corresponds to northern latitudinal region whereas blue presents the southern counterpart. There are several interesting features revealed by latitudinal distribution of annual variation. The annual variations in southern hemisphere at all latitudinal zone follows the solar cycle. The amplitude of annual variations in southern latitudinal zone is higher than corresponding northern region during the considered period. We also note that hemispheric asymmetry, in amplitude of annual variations, decreases from low to high-latitudes. The maximum amplitude of annual variations in the southern regions is 340%, 140% and 114% higher than that of corresponding northern region for low, mid and high-latitudes, respectively. The annual variations at mid and high-latitudes are out of phase in both hemispheres for all years. At low-latitudes, from 2000 to 2005, the northern region annual variations are in phase with southern counterpart and reveals the existence of winter anomaly in northern hemisphere during the period. However, we do not find any annual variation in the northern low-latitude region from 2006 to 2007.

3.3. Morphology of semi-annual variations

As indicated by wavelet power spectrum, there is increase in power of semi-annual periods (about 6 month periodicity) around solar maximum. The present section is aimed to present the morphology of semi-annual variation in both hemispheres at different latitudinal regions. Fig. 6b presents the semi-annual variations extracted using band-pass filter for northern (in red) and southern (in blue) hemisphere. The amplitude of semi-annual variations is in-phase in both hemispheres and intensified around the maximum phase of SC-23 and SC-24. The semi-annual variation in the northern hemisphere is higher than southern counterpart and this effect is enhanced around the maximum phase of solar cycle 23. The maximum amplitude of semi-annual variation in the norther hemisphere (April 2001) is about 10% higher than the corresponding maximum of southern hemisphere. The maximum amplitude of annual variation is about 70% lower in northern hemisphere than maximum amplitude of semi-annual variation in the southern counterpart. This corresponds well to wavelet power spectrum (Fig. 5) which highlights that annual variation dominates in the southern hemisphere whereas semi-annual component dominates in the northern counterpart. Similar to annual variation, semi-annual component is further investigated at high, mid and low-latitudes as depicted in Fig. 9a, 9b and 9c, respectively. The hemisphere asymmetry in the amplitude of semi-annual is maximum at high-latitudes (30% high in northern part), followed by mid-latitudes (17% high in northern part) and minimum at low-latitudes (8% high in northern part). There were no semi-annual variations from August 2007 to March 2009 at high-latitudes. During the deep solar minimum, the amplitude of semi-annual component has reduced, however this reduction is maximum for high-latitudes, followed by mid and low-latitudes, respectively.

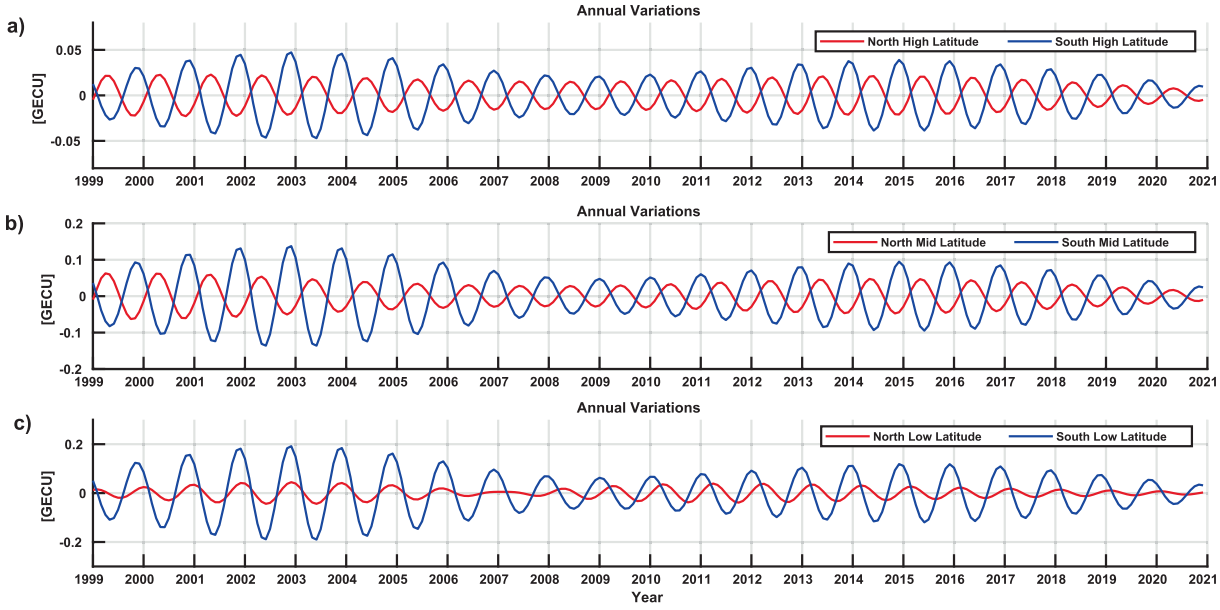

Fig. 8. **a**) Annual variations at northern (in red) and southern (in blue) high latitude region from 1999 to 2020 **b)** same as Fig. 8 (a) but for mid-latitudes **c)** same as Fig. 8 (a) but for low-latitudes.

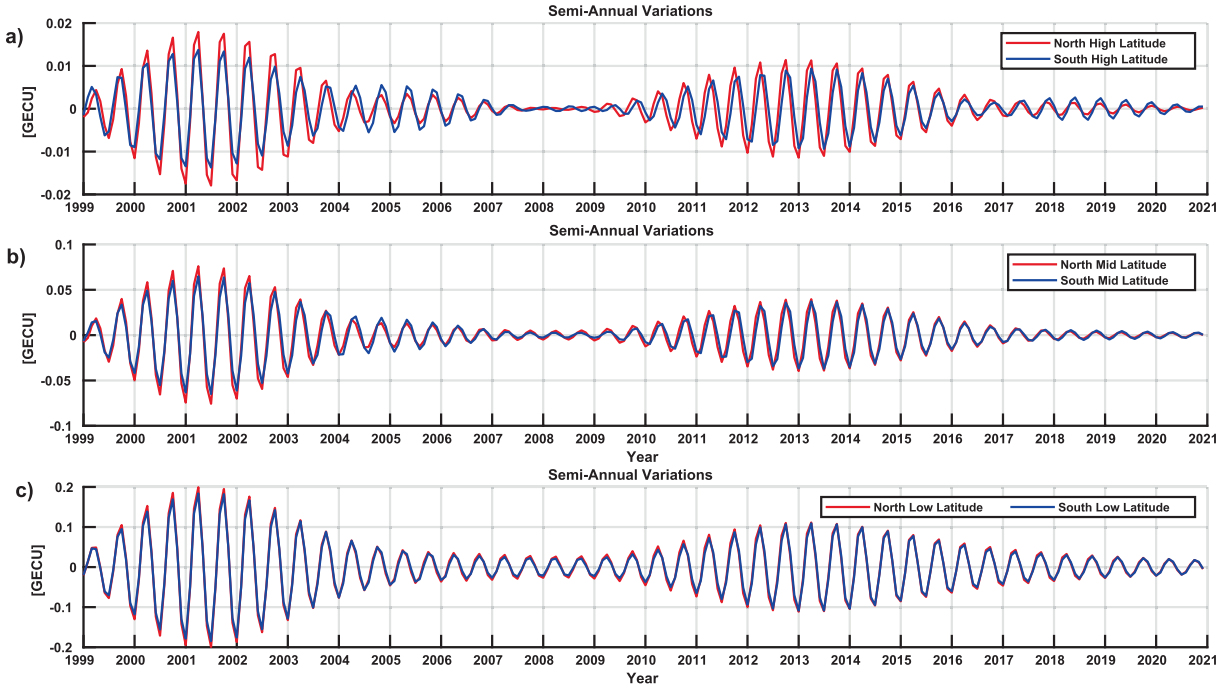

Fig. 9. **a**) Semi-annual variations at northern (in red) and southern (in blue) high latitude region from 1999 to 2020 **b)** same as Fig. 9 (a) but for mid-latitudes **c)** same as Fig. 9 (a) but for low-latitudes.

3.4. The GEC, HEC and REC variation with F10.7 index

Fig. 10(a to i) show the scatter plots of the monthly averaged electron content versus monthly averaged solar radio flux F10.7. A quadratic fitting has been applied to electron content globally and regionally at different latitudes in each hemisphere, the corresponding fitting equation is shown on each subfigure in red bold fonts. Such quadratic fitting has been suggested by many previous studies (Gupta and Singh, 2001; Kouris et al., 1998; Liu et al., 2004; Liu and Chen, 2009). In this regard, Liu and Chen (2009) recommended that the quadratic regression is an optimum choice while describing the effects of a solar activity on ionosphere. The sign of quadratic term in fitting equation describes the possible variation of electron content with increasing F10.7, i.e., a positive sign suggests

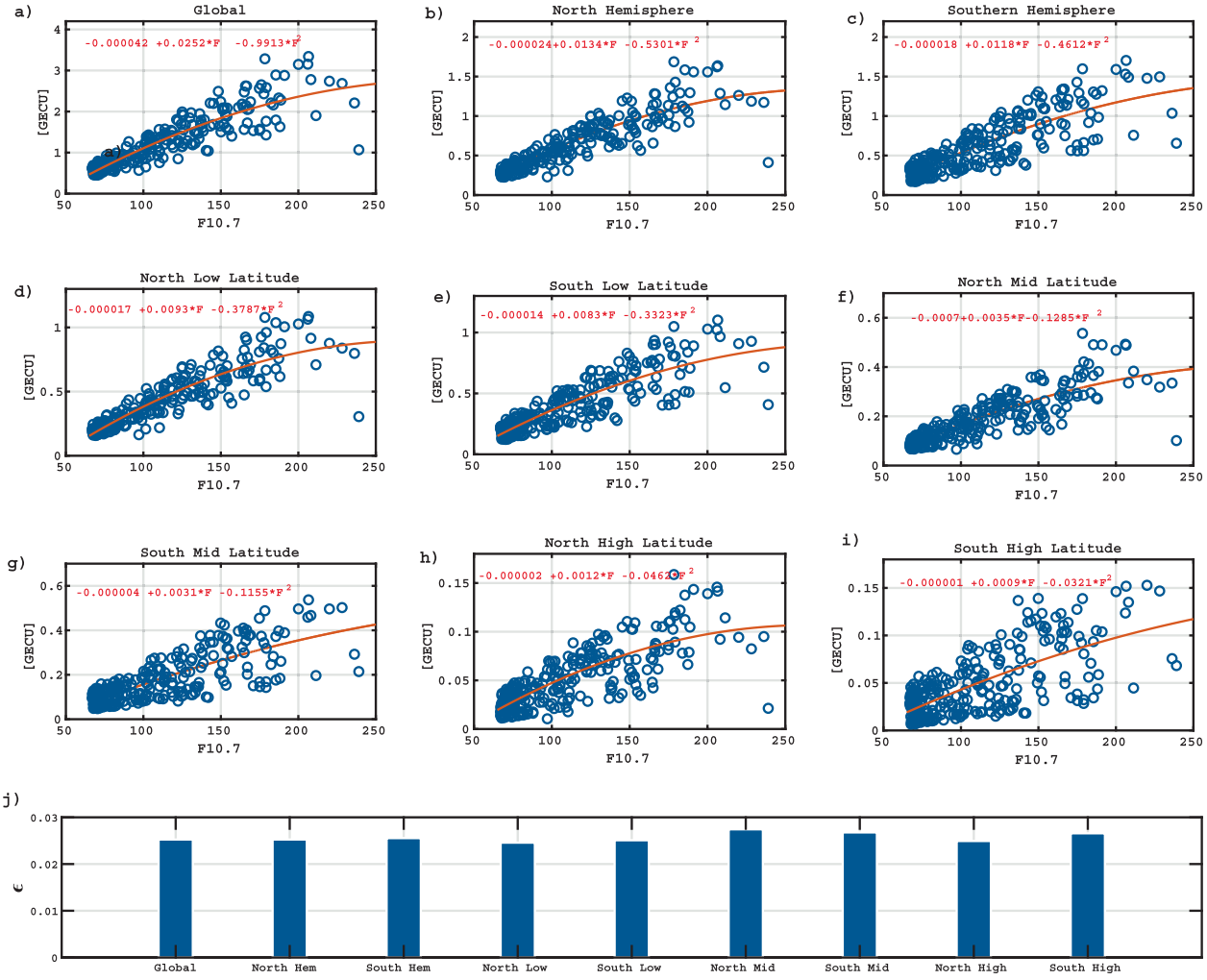

Fig. 10. Scatter plot of monthly averaged electron content versus solar radio flux F10.7 at **a)** globally **b)** in the northern hemisphere, **c)** southern hemisphere **d)** northern low-latitudes **e)** southern low-latitudes **f)** northern mid-latitudes **g)** southern mid-latitudes h) northern high-latitudes **i)** southern high-latitudes. On each figure curve and equation presents quadratic fitting where F in equation corresponds to F10.7. **j)** ratio of linear to quadratic term of fitting at all regions.

amplification and negative values correspond to saturation. All results (Fig. 10(a to i)) show a linear increase in electron content with rise in F10.7 in low solar activity region (F10.7 <150) while for the high solar activity a saturation effect is evident in all regions. This saturation is also confirmed by a negative sign of quadratic term in fitting equation at all respective latitudes. However, the extent of this effect varies with latitudes and to quantify the extend non-linearity at different regions, ratio of linear to quadratic term (epsilon) is calculated and plotted in Fig. 10 (j). Thus, the higher ratio corresponds to higher linearity in variation and vice versa. Fig. 10(j) indicates that mid-latitudes region of each hemisphere depicts a better linear trend with F10.7, followed by high- and low-latitudes regions, respectively. However, response of both hemispheres is found to symmetric at all the sectors. Fig. 11 is similar to Fig. 10 but for electron content and EUV (0.1–50 nm) flux. It can be observed that electron content at different latitudes varies more linearly with EUV flux as compared to F10.7 index. However, there is also a saturation effect detected in the electron content at EUV flux. The ratio of linear and quadratic term of fitting – as depicted in Fig. 11(j) – have much higher values for EUV than F10.7. This shows that saturation effect in EUV flux is much low as compared to F10.7. Moreover, Fig. 11(j) also shows that saturation effect in EUV is maximum at low-latitude region and minimum at northern mid-latitude region.SW.

4. Discussion

The GEC and HEC show that during the maximum of solar cycle 23, the TEC is higher as compared to solar cycle 24. This corresponds well to the low solar activity of the later solar cycle. This quadratic fitting shows that a linear relationship between TEC verses EUV and F10.7 is valid over the periods of low and moderate solar activity. A significant saturation effect is found during the periods of high

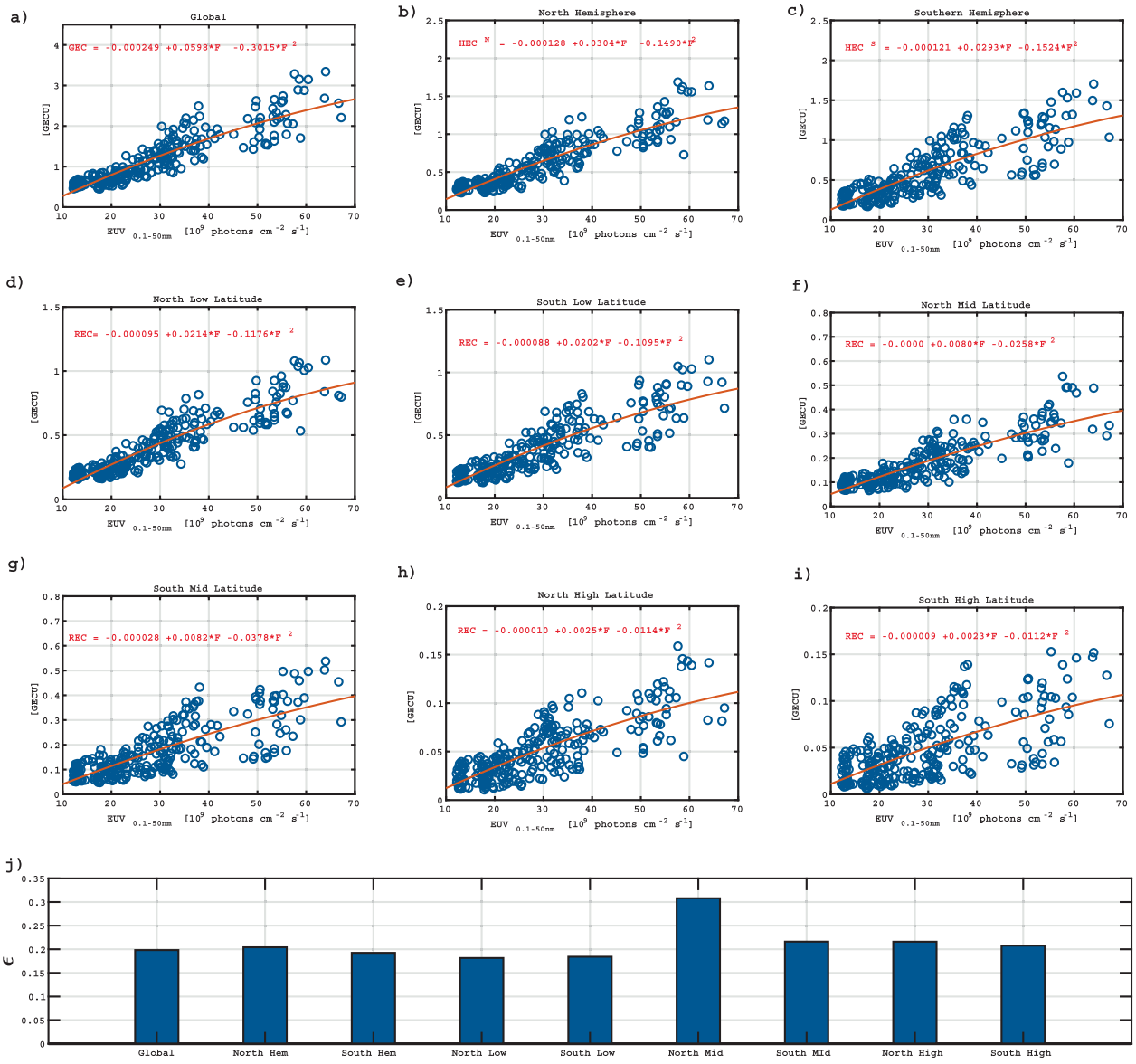

Fig. 11. Similar to Fig. 10 but for monthly averaged electron content verses EUV flux.

solar activity and the extent of saturation is found to be maximum for low-latitudes, followed by high and mid-latitudes. The extent of saturation effect at high solar activity is more pronounced for F10.7 as compared to EUV flux. This saturation effect in the ionospheric plasma density during the period of high solar activity is also reported by many previous studies (Gupta and Singh, 2001; Balan et al., 1994; Richards, 2001; Liu et al., 2006; Liu et al., 2011, Yasyukevich et al., 2018). Balan et al. (1994) argued that non-linear trend between EUV and F10.7 have caused the observed saturation effect in TEC. Afraimovich et al. (2008a) also reported the saturation in GEC with F10.7 index and EUV during high solar activity. Liu et al. (2011) investigated the saturation effects using the regression model and found that equatorial ionization anomaly crust shows clear features of saturation effect. This has also been verified in our study that the deviation from linear trends during high solar activity is more pronounced at low-latitudes in agreement with Liu et al. (2011). It is not well understood whether the saturation of ionospheric plasma density actually exists, or it is the inabilities of different proxy indices (e.g., F10.7 and R) to represent solar ionizing flux at high solar activity. Balan et al., (1994a, 1994b, 1996) reported that there is no saturation effect in the ionospheric parameters (e.g., TEC and NmF2), and the observed trends in plasma density at high solar activity are due to the non-linear variation of EUV radiations against F10.7. On the other hand, Liu et al., 2003 observed the existence of saturation in foF2 against EUV flux having a maximum effect at equatorial latitudes. The equatorial ionization anomaly and pre-reversal enhancement (PRE) are considered to be the main features responsible for the

observed saturation at low latitudes, whereas at mid latitudes it is caused by thermospheric composition and concentration changes (Liu et al., 2021; Liu et al., 2006). In our work, we first found the correlation between electron content and F10.7 cm index (Fig. 10), which indicate the existence of non-linear variations at a high solar activity. However, it is not conclusive if it is a saturation or an inability of the F10.7 index. To further investigate, we have evaluated the correlation between electron content and EUV flux at different latitudes using a quadratic fitting (Fig. 11). Our results indicate that the saturation effect also exist for EUV flux (non-zero coefficient of quadratic term), however its intensity is significantly reduced as compared F10.7 counterpart. The higher electron content in the northern latitudinal zones, as depicted in Fig. 4, can be associated with stronger winter anomaly in the northern hemisphere. Consequently, the yearly averaged electron content generally remains higher in the northern hemisphere with maximum effect at low latitudes. Moreover, this hemispheric asymmetry follows the solar activity and enhanced during the maximum phase of SC (Yasyukevich et al., 2018). In Fig. 5, based on the periodicity, we can easily recognize three main kinds of perturbations: (1) annual, (2) semi-annual and (3) 32-month period oscillations in GEC and HEC. The 32-month periodicity variations can be associated with quasi-biennial oscillation (QBO) (Tang et al., 2014), which are observed around the maximum phase of SC 23 and 24. It is believed that these oscillations as observed in ionosphere are associated with different stratospheric phenomena (Baldwin et al., 2001). The annual variation is most dominating oscillation in southern hemisphere whereas semi-annual is most dominating in the northern counterpart (Figs. 5 and 6). The annual variations as presented in Fig. 6(a) show a solar cycle dependence but with different phases: the southern hemisphere depicts a maximum (minimum) value of such variations – during the considered period – in the month of December (June), these are the regular annual variations. However, the amplitude of these variations in the northern hemisphere is much smaller than the southern counterpart which might be due to winter anomaly and annual asymmetry (Yasyukevich et al., 2018). Moreover, the phase of annual variations (existence of maxima and minima) in the northern hemisphere varies with solar activity. During the minimum phase of a SC, i.e., from 2005 to 2009 and 2017–2020, maxima occur in the months of May-June, whereas minima is observed in Nov-Dec. This also corresponds to the regular annual variations in the northern hemisphere (Fig. 6a). While during the maximum phase of SC, the phase of annual variations shifts towards the months March-April and Sep-Oct corresponding to maximum and minimum values, respectively. This shift in the phase of annual variation in the northern hemisphere can be associated with the intensity of winter anomaly during the maximum phase of a SC (Mikhailov and Perrone, 2011; Yasyukevich et al., 2018). The annual variation of ionospheric total electron content is much stronger in the southern hemispheres for all latitudes (Figs. 6 and 8). Afraimovich et al. (2008b) also reported about 1.7 times higher annual variations in the southern hemisphere as compared to northern counterpart. The northern hemisphere is found to have higher electron content as compared to southern counterpart for all years except during 2011, where electron contents have almost same value in both hemispheres (Fig. 2c). The December to June ratio of GEC is greater than unity for most of the years with the maximum effect observed in 2011, followed by 2014 and 2001 as depicted in Fig. 7a. Furthermore, the winter to summer ratio in the northern hemisphere also exceeds unity in the year 2001 and 2011. This trend corresponds to fact that winter anomaly in the northern hemisphere in 2001 and 2011 was strong enough to reverse the regular annual variation. This hemispheric asymmetry in the amplitude of annual variations is due to collective effects of several physical phenomena. Firstly, the winter anomaly is exceptionally more intense in the northern hemisphere which depresses the regular annual variation in the northern hemisphere (Mikhailov and Perrone, 2011; Yasyukevich et al., 2018). Secondly, the effects of annual asymmetry are in (out of) phase with regular annual variations in southern (northern) hemisphere. This effect causes a further decrement (enhancement) in the regular annual variation in northern (southern) hemisphere (Torr and Torr, 1973; Zhao et al., 2007; Liu et al., 2009; Yasyukevich et al., 2018). The observed asymmetry in the amplitude of annual variation is maximum for the low-latitudes region, followed by mid and high-latitudes regions. At low-latitudes, from 2001 to 2006 the annual variation in northern hemisphere becomes in phase with southern counterpart, i.e. December solstice have higher electron content than June solstice. The winter anomaly during this period was strong enough to reverse the regular annual variations. These results are consistent with the finding of Pavlov and Pavlova (2012) where they reported that intensity of winter anomaly increases from mid to low-latitudes in the northern hemisphere.

The semi-annual variations are in phase in both hemispheres and changes with solar cycle. The amplitude of semi-annual variation in slightly higher in the northern hemisphere, for the considered period, which is evident at different latitudinal zones. This hemispheric difference in the amplitude is minimum at low-latitudes (7%) and maximum at high-latitudes (30%). Rishbeth et al. (2000) and Fuller-Rowell (1998) proposed that thermospheric spoon effect is one of the main mechanisms for such observed semi-annual variation. The solar heating is symmetric in equinoxes and the turbulent mixing is relatively weaker compared to that in solstices which causes higher O/N_2 ratio during equinox than during solstices. Symmetric phase and amplitude of semi-annual variation in both hemispheres at all latitudes suggest strong hemispheric electrodynamics coupling (Liu et al., 2009).

5. Conclusion

We have studied the ionosphere electron content variation by analyzing the GIMs data from 1998 to 2020. In this regard, features of global, hemispheric and regional electron contents in different latitudinal zones are considered. The main findings are summarized as following:

1. The global and regional electron content varies linearly with F10.7 and EUV under low solar activity. However, during the high solar activity a non-linear effect in REC, is observed at all latitudes with a maximum effect in low-latitudes region.
2. The extent of non-linear ~~of~~ effect is more pronounced for F10.7 index as compared to EUV flux.
3. During the peak of solar cycle 23, GEC is about 34% higher than the peak of solar cycle 24, which corresponds to a high EUV for the former cycle.
4. Wavelet power spectrum indicates the existence of annual, semi-annual and 32-month periodicity variations during this period. Moreover, it has been found that semi-annual variations mainly dominate in the northern hemisphere whereas annual variations dominate in southern counterpart.
5. The 32-month period oscillations are observable around maximum phase of solar cycle and might be associated with QBO of stratosphere.
6. The annual variation in electron content is much stronger in the southern hemisphere and varies with phase of a solar cycle. The northern hemisphere exhibits relatively weak annual variation and varies weakly with the solar cycle. The winter anomaly and annual asymmetry reduces the amplitude of regular annual variations with the maximum effect at low-latitudes.
7. The hemispheric asymmetry in the amplitude of semi-annual variations is maximum for low-latitudes, followed by mid and high-latitudes, respectively.
8. The phase difference in annual variation, for both hemispheres at all latitudes except at low-latitudes, have been observed. The annual variation at northern low-latitude becomes in-phase with southern counterpart from 2000 to 2005. This can be associated to existence of strong winter anomaly that reveres the regular annual variations.
9. The semiannual variation is symmetric in both hemispheres and varies with solar cycle. The maximum amplitude of annual variations in northern hemisphere is about 30%, 16% and 8% higher than the corresponding high, mid and low-latitudes of southern hemisphere, respectively.

Declaration of Competing Interest

The authors declare that they have no known competing financial interests or personal relationships that could have appeared to influence the work reported in this paper.

Acknowledgement

This research work was supported by the Higher Education Commission (HEC) of Pakistan through NRPU project No 20-14405/NRPU/R&D/HEC/2021 titled "Space weather effects on ionosphere". The authors are thankful to the IGS Community for providing GNSS data, OMNI web data center (http://omniweb.gsfc.nasa.gov/) for making available solar indices. The SEM/SOHO EUV data are downloaded from the Web site http://www.usc.edu/dept/space_science/semdatafolder/long/. The CELIAS/SEM experiment on the Solar Heliospheric Observatory (SOHO) spacecraft (SOHO is a joint European Space Agency, U.S. National Aeronautics and Space Administration mission). The 10.7 cm solar radio flux data are provided as a service by the National Research Council of Canada. We thank the SDO/AIA instrument team for providing the coronal observations. C. Ammory-Mazaudier thank the ISSI-Bern International Team of 'Why Ionospheric Dynamics and Structure Behave Differently in The African Sector? (The team leaders E. Yizengaw & K. Groves) for a valuable discussion about part of the result that is included in this paper. Authors are thankful to three anonymous reviewers for providing useful suggestion.

References

Afraimovich, E.L., Astafyeva, E.I., Zhivetiev, I.V., 2006. Solar activity and global electron content. Dokl. Earth Sci. 409 (2), 921–924. https://doi.org/10.1134/s1028334x06060195.

Afraimovich, E.L., Astafyeva, E.I., Oinats, A.V., Yasukevich, Y.V., Zhivetiev, I.V., 2008a. Global electron content: a new conception to track solar activity. Ann. Geophys. 26, 335–344. https://doi.org/10.5194/angeo-26-335-2008.

Afraimovich, E.L., Astafyeva, E.I., Zhivetiev, I.V., Oinats, A.V., Yasyukevich, Yu.V., 2008b. Global electron content during solar cycle 23. Geomagnetism and Aeronomy. Pleiades Publishing Ltd. https://doi.org/10.1134/s0016793208020084.

Astafyeva, E.I., Afraimovich, E.L., Oinats, A.V., Yasukevich, Y.V., Zhivetiev, I.V., 2007. Dynamics of global electron content in 1998–2005 derived from global GPS data and IRI modeling. In: Advances in Space Research. Elsevier BV. https://doi.org/10.1016/j.asr.2007.11.007.

Balan, N., Bailey, G.J., Jenkins, B., et al., 1994a. Variations of ionospheric ionization and related solar fluxes during an intense solar cycle. J. Geophys. Res. 99, 2243–2253.

Balan, N., G. J. Bailey, and Y. Z. Su, Variations of the ionosphere and related solar fluxes during solar cycles 21 and 22, Adv. Space Res., 18, (3)11–(3)14, 1996.

Balan, N., G. J. Bailey, and R. J. Moffett, Modeling studies of ionospheric variations during an intense solar cycle, J. Geophys. Res., 99, 17,467–17,475, 1994.

Baldwin, M.P., Gray, L.J., Dunkerton, T.J., Hamilton, K., Haynes, P.H., Randel, W.J., et al., 2001. The quasi-biennial oscillation. Rev. Geophys. https://doi.org/10.1029/1999rg000073. American Geophysical Union (AGU).

Bartels, J., 1932. Terrestrial-magnetic activity and its relations to solar phenomena. J. Geophys. Res. https://doi.org/10.1029/te037i001p00001. American Geophysical Union (AGU).

Berkner, L.V., Wells, H.W., 1938. Non-seasonal change of F2-region ion density. Terr. Magn. Atmos. Electr. 43, 15–36.

Burns, A.G., Wang, W., Qian, L., Solomon, S.C., Zhang, Y., Paxton, L.J., Yue, X., 2014. On the solar cycle variation of the winter anomaly. J.

Geophys. Res. (Space Phys.) 119, 4938–4949. https://doi.org/10.1002/2013JA019552.

Chapman, S., 1931. The absorption and dissociative or ionizing effect of monochromatic radiation in and atmosphere on a rotating Earth: part II. Grazing incidence. Proc. Phys. Soc. 43, 483–501.

Cortie, A.L., 1912. Sun-spots and Terrestrial Magnetic Phenomena, 1898-1911: the Cause of the Annual Variation in Magnetic Disturbances. Monthly Notices of the Royal Astronomical Society. Oxford University Press (OUP). https://doi.org/10.1093/mnras/73.1.52.

Dang, T., Wang, W., Burns, A., Dou, X., Wan, W., Lei, J., 2017. Simulations of the ionospheric annual asymmetry: Sun-Earth distance effect. J. Geophys. Res. Space Physics 122, 6727–6736. https://doi.org/10.1002/2017JA024188.

Fuller-Rowell, T. J. (1998, March 1). The "thermospheric spoon": A mechanism for the semiannual density variation. Journal of Geophysical Research: Space Physics. American Geophysical Union (AGU). https://doi.org/10.1029/97ja03335

Gupta, J.K., Singh, L., 2001. Long term ionospheric electron content variations over Delhi. Ann. Geophys. 18, 1635–1644. https://doi.org/10.1007/s00585-001-1635-8.

Jee, G., Lee, H.-B., Kim, Y.H., Chung, J.-K., Cho, J., 2010. Assessment of GPS global ionosphere maps (GIM) bycomparison between CODE GIM and TOPEX/Jason TEC data: Ionospheric perspective. J. Geophys. Res. 115, A10319. https://doi.org/10.1029/2010JA015432.

Judge, D. et al., 1998. First solar EUV irradiances obtained from SOHO by the SEM. Sol. Phys. 177, 161–173. https://doi.org/10.1023/A:1004929011427.

Kouris, S.S., Bradley, P.A., Dominici, P., 1998. Solar-cycle variation of the daily foF2 and M(3000)F2. Ann. Geophys. 16, 1039–1042.

Liu, L., Chen, Y., 2009. Statistical analysis of solar activity variations of total electron content derived at Jet Propulsion Laboratory from GPS observations. J. Geophys. Res. 114, A10311. https://doi.org/10.1029/2009JA014533.

Liu, L., Chen, Y., Le, H., 2021. Response of the Ionosphere to Varying Solar Fluxes. Upper Atmosphere Dynamics and Energetics. Wiley. https://doi.org/10.1002/9781119815631.ch16.

Liu, Q., Hernández-Pajares, M., Lyu, H., Goss, A., 2021. Influence of temporal resolution on the performance of global ionospheric maps. Journal of Geodesy. Springer Science and Business Media LLC. https://doi.org/10.1007/s00190-021-01483-y.

Liu, L., Luan, X., Wan, W., Lei, J., Ning, B., 2004. Solar activity variations of equivalent winds derived from global ionosonde data. J. Geophys. Res. 109, A12305. https://doi.org/10.1029/2004JA010574.

Liu, L., Wan, W., Ning, B., Pirog, O.M., Kurkin, V.I., 2006. Solar activity variations of the ionospheric peak electron density. J. Geophys. Res. 111, A08304. https://doi.org/10.1029/2006JA011598.

Liu, L., Wan, W., Ning, B., Zhang, M.-L., 2009. Climatology of the mean total electron content derived from GPS global ionospheric maps. J. Geophys. Res. 114, A06308. https://doi.org/10.1029/2009JA014244.

Liu, L., Wan, W., Chen, Y., Le, H., 2011. Solar activity effects of the ionosphere: A brief review. Chin. Sci. Bull. 56 (12), 1202–1211. https://doi.org/10.1007/s11434-010-4226-9.

Liu, J. Y., Y. I. Chen, and J. S. Lin (2003), Statistical investigation of the saturation effect in the ionospheric foF2 versus sunspot, solar radio noise, and solar EUV radiation, J. Geophys. Res., 108(A2), 1067, doi:10.1029/2001JA007543

McIntosh, D.H., 1959. On the annual variation of magnetic disturbances. Phil. Trans. Roy. Soc. London A 251 (1001), 525–552. https://doi.org/10.1098/rsta.1959.001.

Mendillo, M., Huang, C.-L., Pi, X., Rishbeth, H., Meier, R., 2005. The global ionospheric asymmetry in total electron content. J. Atmos Sol. Terr. Phys. 67, 1377–1387.

Mikhailov, A.V., Perrone, L., 2011. On the mechanism of seasonal and solar cycleNmF2variations: A quantitative estimate of the main parameters contribution using incoherent scatter radar observations. J. Geophys. Res.: Space Phys. https://doi.org/10.1029/2010ja016122.

Pavlov, A.V., Pavlova, N.M., 2012. Variations in statistical parameters of the NmF2 winter anomaly with latitude and solar activity. Geomagn. Aeron. 52, 335–343. https://doi.org/10.1134/S0016793212030127.

Ratovsky, K.G., Klimenko, M.V., Yasyukevich, Y.V., Klimenko, V.V., Vesnin, A.M., 2020. Statistical analysis and interpretation of high-, mid- and low-latitude responses in regional electron content to geomagnetic storms. Atmosphere 11 (12), 1308. https://doi.org/10.3390/atmos11121308.

Richards, P.G., 2001. Seasonal and solar cycle variations of the ionospheric peak electron density: Comparison of measurement and models. J. Geophys. Res. Space Phys. 106 (A7), 12803–12819. https://doi.org/10.1029/2000ja000365.

Rishbeth, H., 1998. How the thermospheric circulation affects the ionospheric F2-layer. J. Atmos. Sol. Terr. Phys. 60 (14), 1385–1402.

Rishbeth, H., 2006. F region links with the lower atmosphere? J. Atmos. Sol. Terr. Phys. 68, 469–478.

Rishbeth, H., 2007. Thermospheric targets. Eos, Trans. Am. Geophys. Union 88 (17), 189–193. https://doi.org/10.1029/2007eo170002.

Rishbeth, H., Müller-Wodarg, I.C.F., Zou, L., Fuller-Rowell, T.J., Millward, G.H., Moffett, R.J., Idenden, D.W., Aylward, A., 2000. D.: Annual and semiannual variations in the ionospheric F2-layer: II. Physical discussion. Ann. Geophys. 18, 945–956 http://www.ann-geophys.net/18/945/2000/.

Rishbeth, H., Müller-Wodarg, I.C.F., 2006. Why is there more ionosphere in January than in July? The annual asymmetry in the F2-layer. Ann. Geophys. 24, 3293–3311.

Rösch, A., Schmidbauer, H., 2016. WaveletComp 1.1: A guided tour through the R package. URL: http://www.hsstat.com/projects/WaveletComp/WaveletComp_guided_tour.pdf.

Russell, C.T., McPherron, R.L., 1973. Semiannual variation of geomagnetic activity. J. Geophys. Res. https://doi.org/10.1029/ja078i001p00092. American Geophysical Union (AGU).

Tang, W., Xue, X.-H., Lei, J., Dou, X.-K., 2014. Ionospheric quasi-biennial oscillation in global TEC observations. J. Atmospheric Sol.-Terrestrial Phys. https://doi.org/10.1016/j.jastp.2013.11.002.

Torr, M.R., Torr, D.G., 1973. The seasonal behaviour of the F2-layer of the ionosphere. J. Atmos. Terr. Phys. 35, 2237–2251.

Unnikrishnan, K., Nair, R.B., Venugopal, C., 2002. Harmonic analysis and an empirical model for TEC over Palehua. J. Atmos. Solar-Terr. Phys. 64, 1833–1840.

Wu, C.C., Fryb, C.D., Liu, J.Y., Lioud, K., Tseng, C.L., 2004. Annual TEC variation in the equatorial anomaly region during the solar minimum: September 1996-August 1997. J. Atmos. Solar-Terr. Phys. 66, 199–207.

Yasyukevich, Yu.V., Yasyukevich, A.S., Zhfvetiev, I.V., 2018. Global Electron Content in the 23rd and 24th Solar Cycles. 2018 Progress in Electromagnetics Research Symposium (PIERS-Toyama). IEEE. https://doi.org/10.23919/piers.2018.8597938.

Yasyukevich, Y., Yasyukevich, A., Ratovsky, K., Klimenko, M., Klimenko, V., et al., 2018b. Winter anomaly in NmF2 and TEC: when and where it can occur. J. Space Weather Space Clim. 8, A45.

Zeng, Z., Burns, A., Wang, W., Lei, J., Solomon, S., Syndergaard, S., et al., 2008. Ionospheric annual asymmetry observed by the COSMIC radio occultation measurements and simulated by the TIEGCM. J. Geophys. Res.: Space Phys. 113 (A7), n/a-n/a. https://doi.org/10.1029/2007ja012897.

Zerbo, J.-L., Amory-Mazaudier, C., Ouattara, F., 2012. Geomagnetism during solar cycle 23: Characteristics. J. Adv. Res. https://doi.org/10.1016/j.jare.2012.08.010.

Zhao, B., Wan, W., Liu, L., Mao, T., Ren, Z., Wang, M., Christensen, A. B., 2007. Features of annual and semiannual variations derived from the global ionospheric maps of total electron content. Ann. Geophys. 25, 2513–2527. https://doi.org/10.5194/angeo-25-2513-2007.

Zou, L., Rishbeth, H., Müller-Wodarg, I.C.F., Aylward, A.D., Millward, G.H., Fuller-Rowell, T.J., Idenden, D.W., Moffett, R.J., 2000. Annual and semiannual variations in the ionospheric F2-layer. I. Modelling. Annal. Geophys. 18 (8), 927–944. https://doi.org/10.1007/s00585-000-0927-8.